J. Appl. Phys. in press

A Reduced Moment-Based Model for Precipitation Kinetics and Application to Dopant Activation in Silicon

Iuval Clejan and Scott T. Dunham

Electrical, Computer and Systems Engineering Department,
Boston University, Boston, MA 02215.

Abstract

A moment-based model for the time evolution of extended defect size distributions is introduced as a computationally-efficient method for the quantitative modeling of precipitation processes. Because the model accounts for how the size distribution of aggregates changes with time, it is able to account for thermal history effects that are missed by simpler models. However, by considering only the lowest moments of the distribution, rather than the full distribution itself, the model can be practically applied to nonhomogeneous systems for which it is impractical to include the full distribution at every point in space. The model is tested by implementing it in a process simulator and applying it to the simultaneous diffusion and activation/deactivation of dopants in silicon. Under the conditions compared, we find that the reduced model is nearly equivalent to a previously studied model [S. T. Dunham, *J. Electrochem. Soc.* **142**, 2823 (1995)] maintains the full size distribution and is thus much more computationally intensive. Because the reduced model is derived directly from the more complete model using an energy-minimizing closure assumption, all parameters retain a physical interpretation and the model can be readily extended to a large range of systems.

1 Introduction

Precipitation or aggregation processes play an important role in many materials systems. Because the behavior of precipitates is such a strong function of size, effective modeling of precipitation kinetics requires knowledge of the precipitate size density, which in turn depends on the thermal history of the sample. It is possible to include the effects of precipitate size through following the evolution of the full size distribution [1]. However, this technique is too computationally intensive for most practical applications in spatially nonhomogeneous systems, where a separate solution is required at each point in space. In this work, we present an approach to modeling of precipitation processes that maintains consideration of the precipitate size density and the corresponding connection to fundamental physical parameters, but is much more computationally efficient and thus can be practically applied to a broader range of systems. The model is able to drastically reduce the number of dynamical variables by keeping track of the evolution of only the zeroth, first and second moments of the size distribution (effectively the number of precipitates, their average size and the breadth of the distribution) and using a closure assumption based on minimizing the free energy of the distribution to estimate the full distribution from these moments.

This work was motivated by the need for more fundamental models of processes involving extended defects for the predictive modeling of integrated circuit fabrication processes. For example, at high concentrations, a significant fraction of dopant atoms become inactive due to aggregation into clusters and precipitates. In this work, we only discuss dopant activation/deactivation processes, but the same approach can also be applied to oxygen precipitation during intrinsic gettering and the formation of point defect clusters, dislocation loops and stacking faults following ion implantation, as well as to a wide range of phenomena outside of integrated circuit fabrication processes.

Dopant deactivation is typically modeled using a steady-state solid solubility or clustering model [2, 3]. However, shrinking device feature sizes lead to reduced thermal budgets for integrated circuit processes which make it critical to consider the kinetics of the deactivation process. As an example, arsenic activation has been observed to depend on temperature ramp-down rate [4]. Previous attempts to model deactivation kinetics have generally used dynamic clustering models [4, 5]. Such models are easy to implement in process simulators and can match limited sets of data. However, because clustering models assume a single aggregate size, they cannot account for many of the experimental observations [6, 7, 8, 9, 10], particularly the decrease in sheet resistance (reverse annealing) following a temperature increase.

In a previous paper [1], a model based on explicitly considering the time evolution of the precipitate size distribution was introduced. We will refer to that model as the full kinetic precipitation model, or FKPM. The FKPM was used to match experimental results for activation of implanted and laser annealed box-shaped profiles at low temperatures ($< 800°$C) [6, 7], where profile broadening could be neglected. However, for application to ULSI fabrication process, where profile broadening occurs and the initial shape of the profile is more general, a model is needed which maintains a description of the precipitate size distribution, yet which is more computationally efficient. The use of the moment-based approach described in this paper, which we will call the Reduced Precipitation Model (RPM), leads to a reduction in the number of variables representing the precipitate distribution at each point in space from on the order of 100 to 3, allowing us to reasonably incorporate it in a standard diffusion-reaction solver. We show that the RPM approach appears to be justified because, at least under the conditions considered in this work, it closely reproduces the results of the FKPM.

2 Fundamental Kinetic Equations

The kinetic equations describing the evolution of dopant density and cluster size distribution were discussed in a previous paper [1]. They are reproduced here in order to fix our notation and for easy reference. We will use the convention that sums over n are sums over precipitate size and hence go from $n = 2$ to the largest precipitate size in the system.

$$\frac{dC_A}{dt} = \nabla \cdot (hD\nabla C_A) - 2I_1 - \sum I_n \tag{1}$$

$$\frac{df_n}{dt} = I_{n-1} - I_n \quad (n \geq 2), \tag{2}$$

where C_A is the dopant concentration, D is the dopant diffusivity, h is electric field enhancement term ($h \cong 2$ for the high doping concentrations at which dopant precipitation takes place) [11], and f_n is the concentration of precipitates of size n. The net flux from precipitate size n to $n+1$ due to growth/dissolution processes is

$$I_n = g_n f_n - d_{n+1} f_{n+1}, \tag{3}$$

where g_n and d_n are growth and dissolution rates respectively for a precipitate of size n.

These equations describe the microscopic situation when the fundamental reaction step is a precipitate growing (shrinking) by absorbing (desorbing) a single dopant atom. Thus, the population of precipitates of size n can grow due to either the precipitates of size $n+1$ shrinking or precipitates of size $n-1$ growing. Assuming first order reaction and diffusion processes leads to expressions for the growth and dissolution rates in terms of the dopant density:

$$g_n = D\alpha_n C_A \tag{4}$$

$$d_n = D\beta_n. \tag{5}$$

The exact form of α_n and β_n, depends on what further approximations are made concerning the diffusion field around each precipitate [1] and the relationship between the interface reaction rate (k_n) and the diffusivity. The approximations that we implement in this work are that the diffusion field around each precipitate is the same as would occur under quasi-steady state conditions and that the interface reaction is diffusion-limited, so that $k_n = D/\lambda$ (λ is the hopping distance). However, the moment-based reduction that we present in the next section applies much more generally. The resulting model has

$$\alpha_n = \frac{A_n}{r_n + \lambda} \tag{6}$$

and

$$\beta_{n+1} = \alpha_n C_n^*, \tag{7}$$

where A_n is the surface area of a spherical precipitate with n dopant atoms, r_n is its radius, and C_n^* is the interface concentration of dopants which keeps a precipitate of size n in equilibrium, tending neither to grow nor to shrink.

C_n^* is given by the maximum with respect to the dopant density of the free energy of a precipitate:

$$\Delta G_n = -nkT \log\left(\frac{C_A}{C^{ss}}\right) + \Delta G^{\mathrm{exc}}. \tag{8}$$

Here C^{ss} is the solid solubility of the dopant, and ΔG^{exc} is the excess free energy due to the finite precipitate size and includes the interface and strain energies. We assume for the excess free energy of a precipitate

$$\Delta G_n^{\mathrm{exc}} = c_1 n^{2/3} + c_2 n^{1/3} + c_3 n^{-1}, \tag{9}$$

where the first term corresponds to the dependence of the surface area on size for a precipitate which maintains its aspect ratios as it grows, and the other terms are corrections for the deviation of the free energy from this ideal behavior at small sizes.

For the dopant diffusivity, we assume that

$$D = D_0 + D_-\left(\frac{n}{n_i}\right) + D_H\left(\frac{C_A}{3.3\times 10^{20}\mathrm{cm}^{-3}}\right)^{n_H}, \tag{10}$$

where D_0 and D_- are temperature activated diffusivities with neutral and negatively-charged point defects taken from previously published work on arsenic [12] and phosphorus [13] diffusion, while D_H and n_H account for the interactions of vacancies with multiple dopants at the very high doping densities [14]. For arsenic, experimental values of D_H and n_H are used [15], while no experimental results are available for phosphorus, so n_H is assumed to be the same as for arsenic and D_H remains a model parameter.

3 Reduced Moment-Based Model

We will proceed in analogy with methods used for carrier or fluid transport. Just as it is possible to go from a Boltzmann equation to simpler hydrodynamic equations by computing moments and introducing a closure assumption [16], we seek a description of our system which is simpler than the full kinetic equations. The critical requirement is that we must be able to describe the f_n as functions of a relatively small number of moments. As we will show later, we find that the distribution is well described by its lowest three moments:

$$m_0 = \sum f_n \tag{11}$$

$$m_1 = \sum n f_n \tag{12}$$

$$m_2 = \sum n^2 f_n. \tag{13}$$

The zeroth and first moments correspond to the density of precipitates and the density of precipitated atoms respectively, and the second moment can be related to the standard deviation of the distribution. The ratio of the first to zeroth moment also corresponds to the average size of the precipitates.

If we compute the evolution of the dopant density and the moments from Eqs. (1) and (2), we get a set of equations in terms of sums over the normalized precipitate distribution ($\hat{f}_n$):

$$\frac{dC_A}{dt} = \nabla \cdot (hD\nabla C_A) - 2I_1 - Dm_0(C_A\gamma_2 - \gamma_3) \tag{14}$$

$$\frac{dm_0}{dt} = I_1 \tag{15}$$

$$\frac{dm_1}{dt} = 2I_1 + Dm_0(C_A\gamma_2 - \gamma_3) \tag{16}$$

$$\frac{dm_2}{dt} = 4I_1 + Dm_0(C_A\gamma_4 - \gamma_5) \tag{17}$$

where

$$I_1 = D(\alpha_1 C_A^2 - \beta_2\gamma_1 m_0) \tag{18}$$

$$\gamma_1 = \hat{f}_2 \tag{19}$$

$$\gamma_2 = \sum \hat{f}_n \alpha_n \tag{20}$$

$$\gamma_3 = \sum \hat{f}_{n+1}\beta_{n+1} \tag{21}$$

$$\gamma_4 = \sum \hat{f}_n \alpha_n (2n+1) \tag{22}$$

$$\gamma_5 = \sum \hat{f}_{n+1}\beta_{n+1}(2n+1) \tag{23}$$

$$\hat{f}_n = \frac{f_n}{\sum f_n} = \frac{f_n}{m_0}. \tag{24}$$

As long as the distribution can be well described by its lowest three moments, then the γ_i depend only on $\hat{m}_1 \equiv m_1/m_0$ and $\hat{m}_2 \equiv m_2/m_0$, and the α_n and β_n which depend on temperature and the free energy parameters, but not the doping density or precipitate distribution.

Since any finite number of moments is insufficient to describe an arbitrary distribution, it is necessary to add a closure assumption in order to determine f_n. In this work, we will assume that the precipitate size distribution is the one that minimizes the Gibbs free energy, constrained such that the population of precipitates has the known values of m_0, m_1 and m_2. As long as the moments of the distribution are slowly varying, local growth and shrinkage of precipitates will result in the free energy of the distribution being minimized given the moment values. This is particularly effective for the population of sub-critical precipitates, where as long as the classical nucleation rate is small, only the solute density needs to be slowly varying to accurately estimate this portion of the distribution. The approach can be thought of as a generalized version of Becker-Döring nucleation theory [17].

At very short times, particularly when there is a large dopant supersaturation so that the critical size is very small, we cannot expect a quasi-steady state distribution to have developed, as the moments are changing very rapidly. However, because we have a discrete distribution, the distribution is still accurately described in this regime as long as the values of $\hat{m}_1$ and $\hat{m}_2$ are small so that the distribution is dominated by very small sizes. For example, if the concentration of sizes larger than four is negligible compared to sizes two, three and four, we have three unknowns (f_2, f_3 and f_4) and the three equations defining the lowest three moments. This situation occurs in the early stages of the annealing of laser-annealed profiles, leading to very close agreement between the RPM and the FKPM.

Applying our closure assumption, we are led to minimizing the quantity:

$$\begin{aligned}\Delta G_{Total} &= \sum f_n \Delta G_n + kT f_n \log(f_n/C_S) - kT\eta_0\left(\sum f_n - m_0\right) \\ &\quad - kT\eta_1\left(\sum n f_n - m_1\right) - kT\xi_2\left(\sum n^2 f_n - m_2\right), \qquad (25)\end{aligned}$$

where the second term is the entropy of mixing for the precipitates (C_S is the silicon atom density), and η_0, η_1 and ξ_2 are Lagrange multipliers enforcing the constraints. The resulting distribution is

$$f_n = K\exp(-\Delta G_n/kT + \eta_1 n + \xi_2 n^2), \qquad (26)$$

where $K = C_S\exp(\eta_0 - 1)$.

Because we must have a finite number of precipitates and precipitated atoms, it can be seen that ξ_2 must be negative. Since the number of precipitated atoms is fixed by the value of m_1, the precipitate size distribution cannot depend on C_A. This follows from conservation of material, since any interaction with precipitates that changes C_A also changes m_1. There is of course an indirect dependence on C_A since the evolution of the moments is tightly coupled to the evolution of C_A. In order for f_n to be independent of C_A, we must have

$$\eta_1 = \xi_1 - \log\left(\frac{C_A}{C^{ss}}\right) \qquad (27)$$

with ξ_1 independent of C_A. We can therefore write

$$f_n = K\exp(-\Delta G_n^{\text{exc}}/kT + \xi_1 n + \xi_2 n^2), \qquad (28)$$

where and K, ξ_1 and ξ_2 are independent of C_A. To determine the dependence of K, ξ_1 and ξ_2 on m_0, $\hat{m}_1$ and $\hat{m}_2$, we simply apply Eq. (28) in their definitions to get

$$\hat{m}_1 = \frac{\sum n\exp(-\Delta G_n^{\text{exc}} + \xi_1 n + \xi_2 n^2)}{\sum \exp(-\Delta G_n^{\text{exc}} + \xi_1 n + \xi_2 n^2)}, \qquad (29)$$

$$\hat{m}_2 = \frac{\sum n^2\exp(-\Delta G_n^{\text{exc}} + \xi_1 n + \xi_2 n^2)}{\sum \exp(-\Delta G_n^{\text{exc}} + \xi_1 n + \xi_2 n^2)}, \qquad (30)$$

$$K = m_0 / \sum \exp(-\Delta G_n^{\text{exc}} + \xi_1 n + \xi_2 n^2). \qquad (31)$$

Thus to calculate f_n given $\hat{m}_1$ and $\hat{m}_2$, we have to solve the two equations Eqs. (29) and (30) for ξ_1 and ξ_2 and then solve Eq. (31) for K.

Solving the nonlinear system given by Eqs. (29) and (30) requires iterative techniques and thus is computationally expensive. Since ξ_1 and ξ_2 are only intermediate variables, and we are ultimately interested in the fluxes appearing on the right hand sides of Eqs. (14) – (17), we can proceed as follows. Before the simulation begins, from ξ_1, ξ_2 sets we generate values of $\hat{m}_1$, $\hat{m}_2$, as well as corresponding γ_i values. We use these values to form a two dimensional table containing discrete $\hat{m}_1$, $\hat{m}_2$ pairs as input variables and the γ_i as output variables. Note that we do not need to calculate K when generating the table, since K cancels out from the γ_i, $\hat{m}_1$ and $\hat{m}_2$. Although the table generation is a relatively slow process, it has to be done only once for each temperature. During a simulation we interpolate from this table the values of the γ_i for each $\hat{m}_1$ and $\hat{m}_2$ that we encounter. Of course once tables for a sufficient set of temperatures have been calculated, it is also possible to interpolate from the resulting three dimensional table.

Because the RPM requires only three solution variables to describe the precipitate distribution at each point in space, it is suitable for integration into a process simulator based on the solution of continuity equations. We have implemented the RPM along with concentration-dependent dopant diffusion in PEPPER, a one dimensional process simulator with the ability to solve arbitrary sets of partial diferential equations ("dial-an-operator") [18]. We are thus able to simulate precipitation behavior in nonhomogeneous systems and at high temperatures, where substantial profile broadening takes place. Because the precipitated material is assumed to be immobile as well as inactive, the moments of the distribution at each point in space evolve due only to the local concentration of substitutional dopant atoms, which diffuse with a concentration-dependent diffusivity given by Eq. (10).

4 Comparison of Reduced Model to Full Model and Experiment

The ability of the RPM to model the evolution of the full precipitate size distribution using only the the zeroth, first and second moments relies on how accurately the distribution given by these moments along with the closure assumption matches the full distribution. As a test of our approach (and particularly the closure assumption chosen) we ran the FKPM using a variety of time and temperature schedules, extracted the moments of the resulting precipitate distributions and from those moments constructed the distributions assumed by the RPM. As described above, the moments are used to solve for K, ξ_1 and ξ_2 from Eqs. (29), (30) and (31), and those parameters are used in Eq. (28) to give the assumed distribution. Figure 1 shows an example of that comparison for an initial fully-activated (laser-annealed) arsenic concentration of 1.5×10^{21} and an annealing schedule consisting of 32 h at 650°C, followed by an additional 15 minutes at 750°C. As can be seen, although the profile shapes are very distinctive and clearly non-Gaussian, the two distributions are almost identical, demonstrating the effectiveness of minimizing the free energy of the distribution as a closure assumption. We find similar agreement for other annealing conditions.

In order to compare the RPM to both experimental measurements, as well as the FKPM on which it is based, we use model parameters based on optimizing the FKPM model to arsenic and phosphorus activation/deactivation behavior at temperatures below 800°C, where profile broadening can be neglected. The resulting parameters are given in Table I. Note that the two models share parameters as well as basic model assumptions, with the RPM differing only in that the distribution is described by its lowest moments, rather than being given explicitly. Because of this direct correspondence, it is straightforward to incorporate any modifications in the full model directly into the reduced model.

The experimental results considered in this work are from Nobili *et al.* [6, 7], Rousseau *et al.* [10] and Luning *et al.* [19]. In all the experiments, the dopant was initially completely activated by a laser anneal, providing a consistent set of initial conditions. For the FKPM, the density for all sizes except single atoms are set equal to zero, while for the RPM the initial conditions used were

$$\begin{aligned} C_A &= C_{\text{measured}} \\ m_0 &\approx \epsilon \\ m_1 &\approx 2 * m_0 \\ m_2 &\approx 4 * m_0 \end{aligned}$$

where ϵ is a small number. The simulation results were insensitive to the value of ϵ, as long as $\epsilon < 10^5 \text{cm}^{-3}$. The initial conditions on m_1 and m_2 imply that only precipitates of size two are present. The initial condition on m_0 implies that there is a small concentration of these (size 2) precipitates, which is physically reasonable and mathematically necessary in order for the normalized variables $\hat{m}_1$ and $\hat{m}_2$ to vary continuously even at the initial time.

As a first set of comparisons, we look at relatively low temperatures (< 800°C), where broadening of the profile can be neglected and thus the RPM and FKPM can be directly compared. The depth profiles are assumed to be box-shaped (uniform doping up to the melt depth and then negligible below), so only the active doping level in the surface region changes with annealing. In Figure 2, both the RPM and the FKPM are compared with data from Nobili *et al.* [7] in which a heavily phosphorus-doped and laser-annealed wafer is annealed for 1 h at each of a series of temperatures from 300 to 750°C. For these conditions, the RPM almost exactly reproduces the FKPM and both models match the experimental data quite closely.

In Figure 3, we show a comparison of phosphorus activation data from a two step annealing experiment by Nobili *et al.* [7] with the RPM and FKPM. Again, the reduced model gives very similar results to the FKPM, and actually does a slightly better job fitting the experimental data, although the parameters were chosen to optimize the fit of the FKPM. A possible reason for the improved match of the RPM to the experimental results is that the precipitate size distribution is able to (unphysically) change instantaneously in the reduced model to adjust to the new energy minimizing distribution when the temperature is changed, whereas it cannot do so in the FKPM model. This may effectively compensate somewhat for the transient behavior of the diffusion field in the neighborhood of the precipitate, which is ignored due to the steady-state approximation used in this work. Note that both the RPM and the FKPM initially show reverse annealing when the temperature is increased. This behavior is observed experimentally for both phosphorus [7] and arsenic [6, 10], but is inconsistent with the predictions of dynamic clustering models [1].

In Figure 4 we show a comparison of arsenic activation during a 15 minute RTA anneal of arsenic at 800°C from Luning *et al.* [19] to the RPM and FKPM. Again there is a good match to the data and both models agree quite closely, all showing very rapid initial deactivation, followed by much slower precipitation closer to the solubility limit. For such short times, any profile broadening could be considered negligible as it was not resolvable by SIMS [19].

Next, using the same model and parameters, we apply the RPM at higher temperatures and longer times, where diffusion is significant. Figure 5 shows the simulated active and chemical concentrations, along with the precipitate density after 3 hours at 800°C. The initial profile is assumed to be box-shaped due to laser anneal [19], with a depth measured by SIMS. However, since there appears to be substantial SIMS broadening in the measurements, the simulated profiles were convolved with the SIMS response. The SIMS impulse response was assumed to be a one sided (positive side) decaying exponential due to knock-ons. The length parameter in the exponential (effectively the SIMS resolution) was chosen so that the convolution of the impulse response with a box-like Arsenic distribution matched the initial SIMS profile. As can be seen, the simulations show a kink in the chemical composition, coinciding with the position of the edge of the initial profile. To the left of the kink, the dopants rapidly precipitate and act as a source of atoms at a concentration slightly above the solid solubility. The active dopants diffuse into substrate, giving the kink and leading to a broadening of the profile. Although no data is available for direct comparison, similar behaviour (a kink above the solid solubility) had been observed in other experiments with more complicated annealing conditions [20].

At higher temperatures, the extent of profile broadening is much greater. In Figure 6, we compare the results of a simulation of an 8 minute RTA of arsenic at 1000°C with the measured chemical profile [10]. As mentioned above, the parameters used in the simulation are from the optimization of the 15 minute RTA at 800°C. The simulation does an excellent job of matching the SIMS, both in the highly doped region where precipitation occurs, and in the region where the doping is lower and diffusion occurs.

5 Conclusions

We have implemented a reduced, moment-based model for precipitation kinetics which includes a physically sound mechanism for describing the evolution of the precipitate size distribution. We have applied the model to dopant activation/deactivation and successfully incorporated it in a one-dimensional diffusion simulator. The model agrees well with experimental observations and is able to duplicate the results of a previous model [1], while greatly reducing the number of variables required, with a corresponding reduction in the computational resources required.

Because the approach described in this work provides a framework for direct derivation of the reduced model from a model which explicitly considers the full size distribution, it is straightforward to apply the technique to other problems or to modify the assumptions made to consider for example, different dependences of precipitate energy on size or precipitate shapes other than spherical. Since recent work has shown the importance of interactions of point defects with dopant precipitation [21, 22], work is currently under way to extend the RPM to account for the incorporation of point defects into precipitates.

6 Acknowledgements

This work was supported by SRC/SEMATECH. Thanks to Paul Rousseau for providing additional information on experimental results.

References

[1] S. T. Dunham, in **Semiconductor Silicon/1994**, H. Huff, W. Bergholz, and K. Sumino, eds. (Electrochem. Soc. Proc. **94-10**, Pennington, NJ 1994) p. 711.

[2] M. E. Law and R. W. Dutton, *IEEE Trans. CAD* **7**, 181 (1988).

[3] W. Jungling, S. Selberherr, E. Guerrero and H. Potzl, *IEEE Trans. Elec. Dev.* **2**, 156 (1985).

[4] M. Orlowski, R. Subrahmanyan and G. Huffman, *J. Appl. Phys.* **71**, 164 (1992).

[5] M. Y. Tsai, F. F. Morehead and J. E. E. Baglin, *J. Appl. Phys.* **51**, 3230 (1980).

[6] D. Nobili, A. Carabelas, G. Celotti and S. Solmi, *J. Electrochem. Soc.* **130**, 922 (1983).

[7] D. Nobili, A. Armigliato, M. Finetti and S. Solmi, *J. Appl. Phys.* **53**, 1484 (1982).

[8] G. Masetti, D. Nobili and S. Solmi, in **Semiconductor Silicon**, H. R. Huff and E. Sirtl eds. (Electrochemical Society Proc. **77-2**, Pennington, NJ, 1977) p. 648.

[9] P. Negrini, D. Nobili and S. Solmi, *J. Electrochem. Soc.* **122**, 1254 (1975).

[10] P. M. Rousseau, P. B. Griffin, P. G. Carey and J. D. Plummer, in **Process Physics and Modeling**, G. R. Srinivasan, K. Taniguchi and C. S. Murthy eds. (Electrochem. Soc. Proc. **93-6**, Pennington, NJ, 1993) p. 130.

[11] P. M. Fahey, P. B. Griffin and J. D. Plummer *Rev. Mod. Phys.* **61**, 289 (1989).

[12] R. Fair, and M. Y. Tsai, *J. Electrochem. Soc.* **124**, 1107 (1977).

[13] F. Wittel and S. T. Dunham, *Appl. Phys. Lett.* **66**, 1415 (1995).

[14] C. Wu and S. T. Dunham, *J. Appl. Phys.* **78**, 2362 (1995).

[15] A. Nylandsted Larsen, K. K. Larsen, P. E. Andersen, and B. G. Svensson *J. Appl. Phys.* **73**, 691 (1993).

[16] K. Huang, **Statistical Mechanics**, (John Wiley & Sons, New York, 1963).

[17] R. Becker and W. Döring, *Ann. Phys.* **24**, 719 (1935).

[18] B. Mulvaney, W. B. Richardson and T. L. Crandle, *IEEE Trans. Comp. Aid. Des.* **8**, 336 (1989).

[19] S. Luning, P. M Rousseau, P. B Griffin, P. G. Carey, and J. D. Plummer, *IEDM Tech. Dig.*, 457 (1992).

[20] D. Nobili, S. Solmi, A. Parisini, M. Derdour, A. Armigliato, and L.Moro, *Phys. Rev. B* **49**, 2477 (1994).

[21] R. Subrahmanyan, M. Orlowski and A. R. Sitaram, in **Process Physics and Modeling**, G. R. Srinivasan, K. Taniguchi and C. S. Murthy eds. (Electrochem. Soc. Proc. **93-6**, Pennington, NJ, 1993) p. 120.

[22] P. M. Rousseau, P. B. Griffin and J. D. Plummer *IEDM Tech. Dig.*, 861 (1994).

Figure Captions

FIG. 1. Comparison of precipitate size distribution (# of dopant atoms) from FKPM simulation to profile with the same zeroth, first and second moments calculated using the closure assumption of the RPM.

FIG. 2. Peak active phosphorus concentration following each step of a series of one hour anneals. The sample was initially implanted and laser annealed resulting in a box-like profile. The reduced model is nearly indistinguishable from steady state model. Data from Nobili *et al.* [6].

FIG. 3. Peak active phosphorus concentration versus time for a two step anneal. Initial sample was implanted and laser annealed. The samples were annealed first at 550°C for 6 h and then the temperature was changed to 650°C. Data from Nobili *et al.* [6].

FIG. 4. Active arsenic concentration versus time for 15 min anneal at 800°C assuming no diffusion of the profile and box-shaped initial profile. Comparison of experimental results from Luning *et al.* [19] to FKPM and RPM.

FIG. 5. Active and total (chemical) arsenic concentration profiles after a 3 h anneal at 800°C based on simulation of simultaneous diffusion and precipitation. Also shown is the precipitate density and the solid solubility. Simulated profiles were convolved with the calculated SIMS response.

FIG. 6. Active and total (chemical) arsenic concentration profiles after an 8 min RTA at 1000°C based on simulation of simultaneous diffusion and precipitation using the RPM. Also shown is the precipitate density and the solid solubility. Initial and final experimental profiles are from Rousseau *et al.* [10]. Simulated profiles were convolved with the calculated SIMS response.

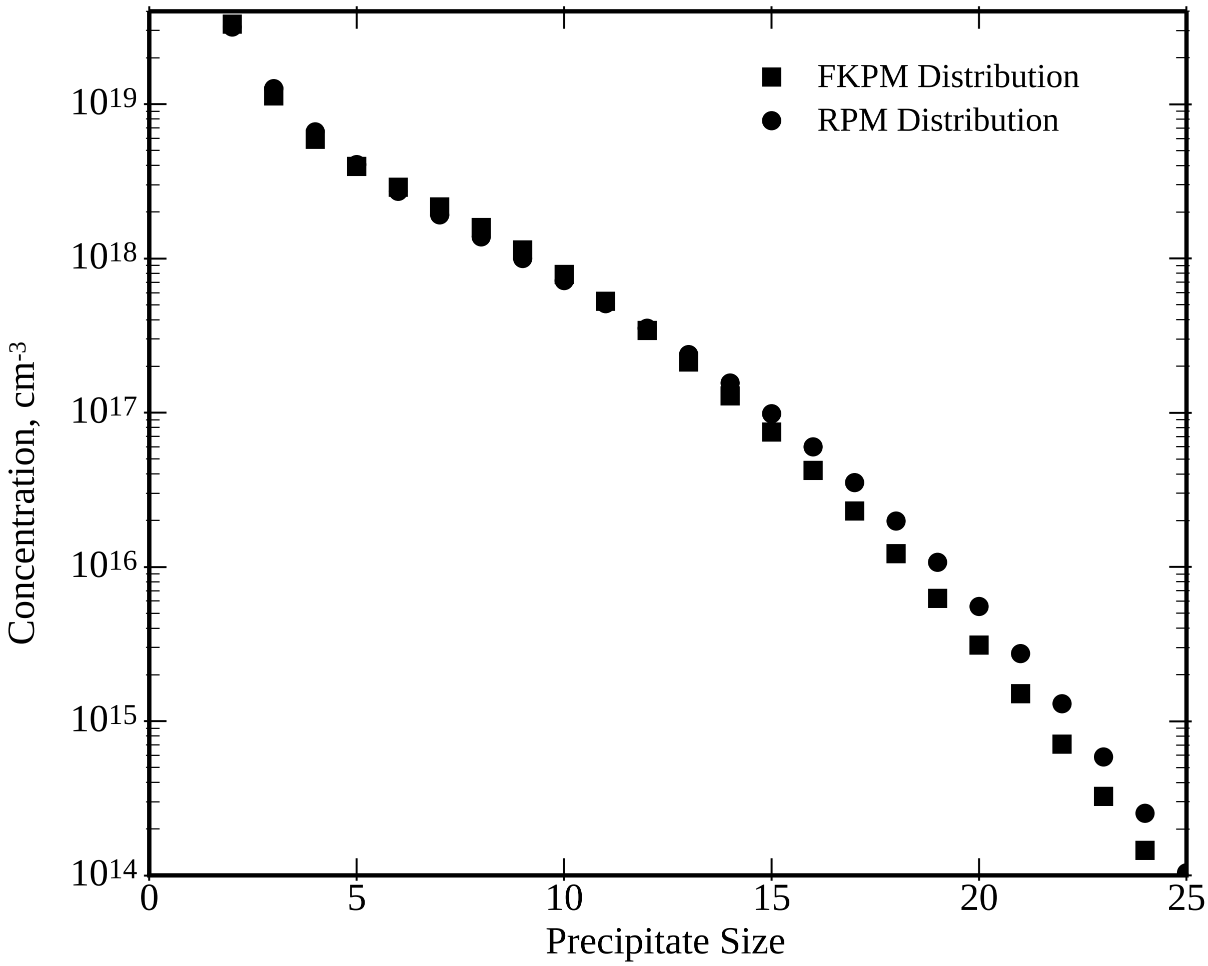

Figure 1: Clejan and Dunham

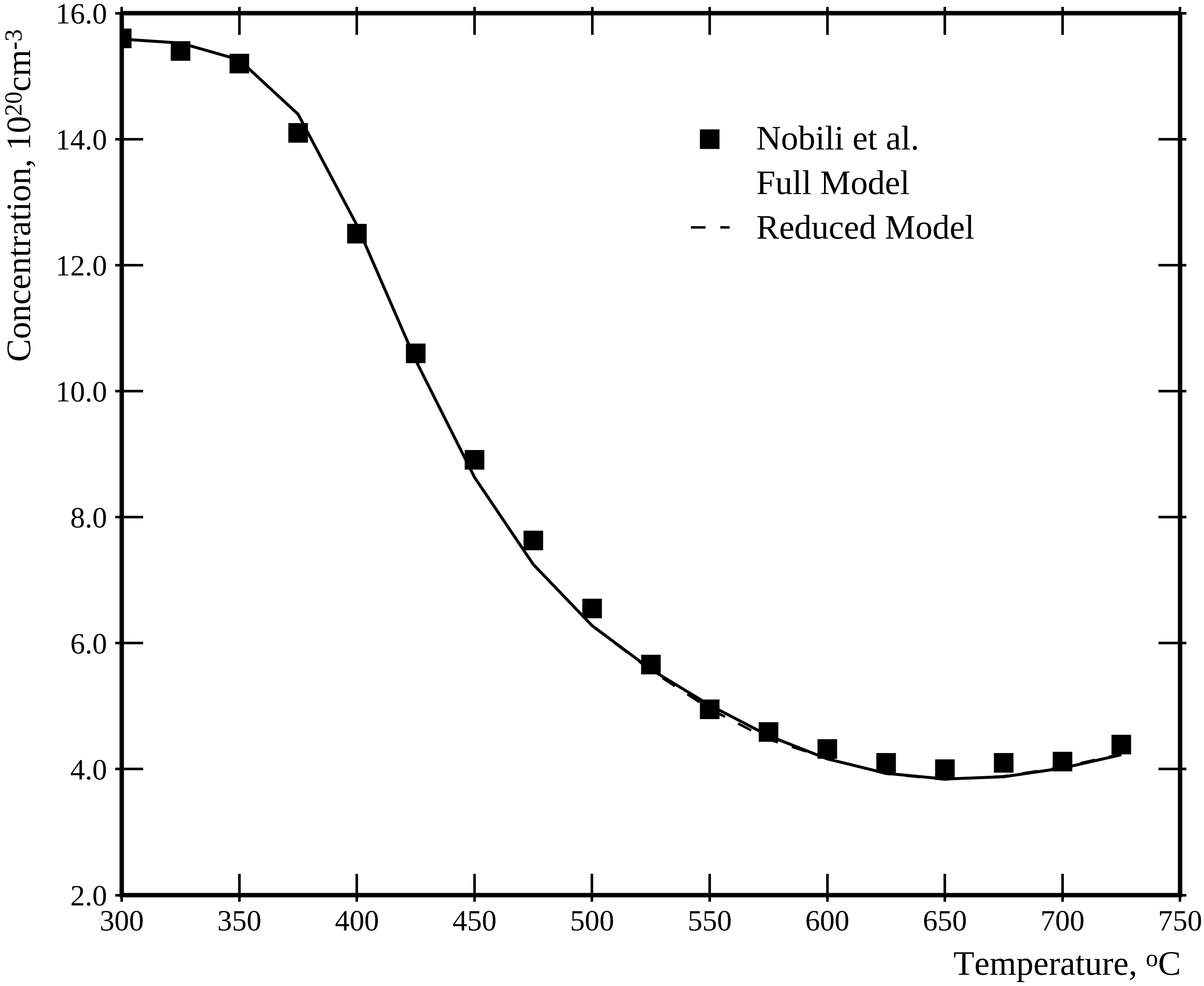

Figure 2: Clejan and Dunham

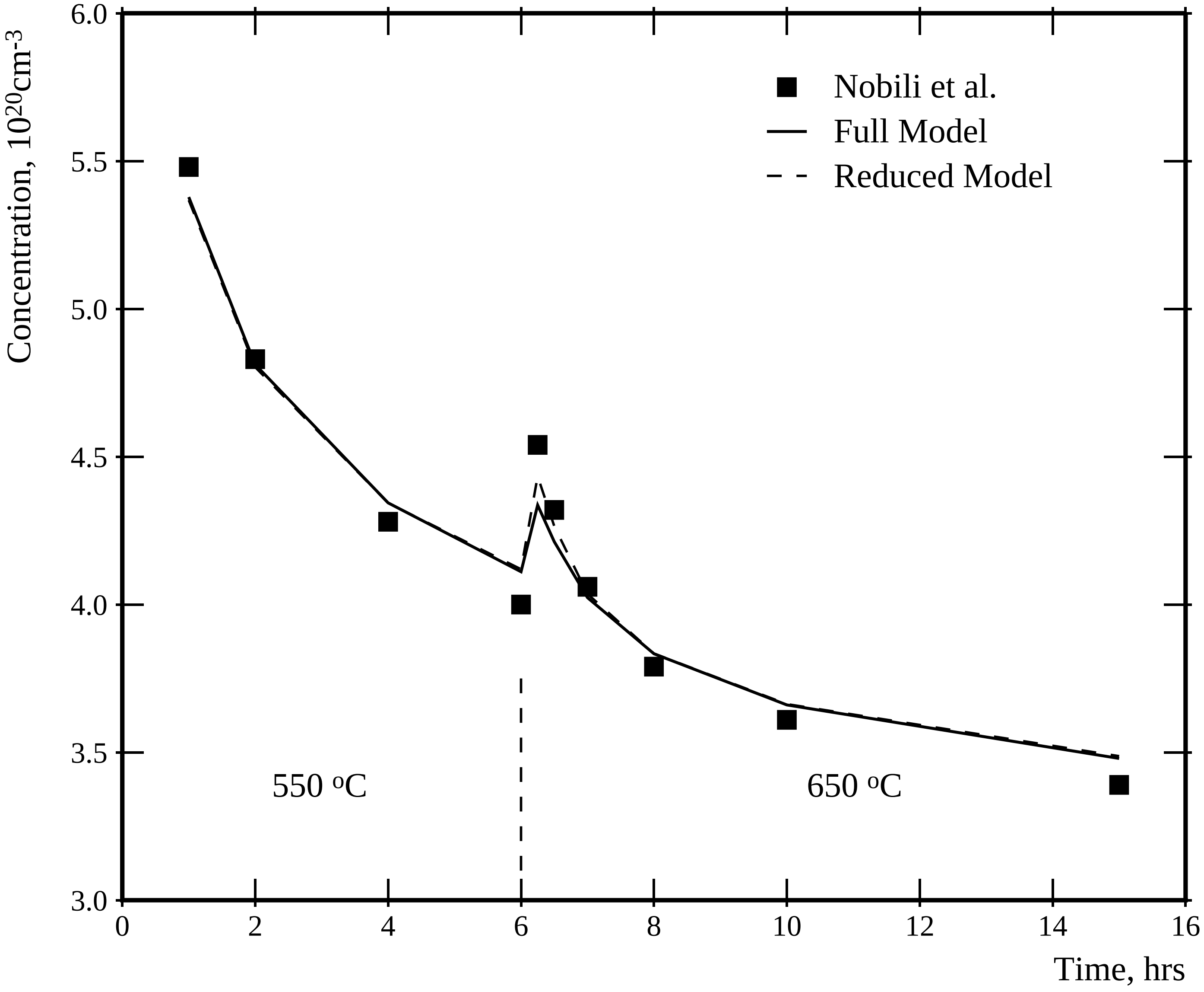

Figure 3: Clejan and Dunham

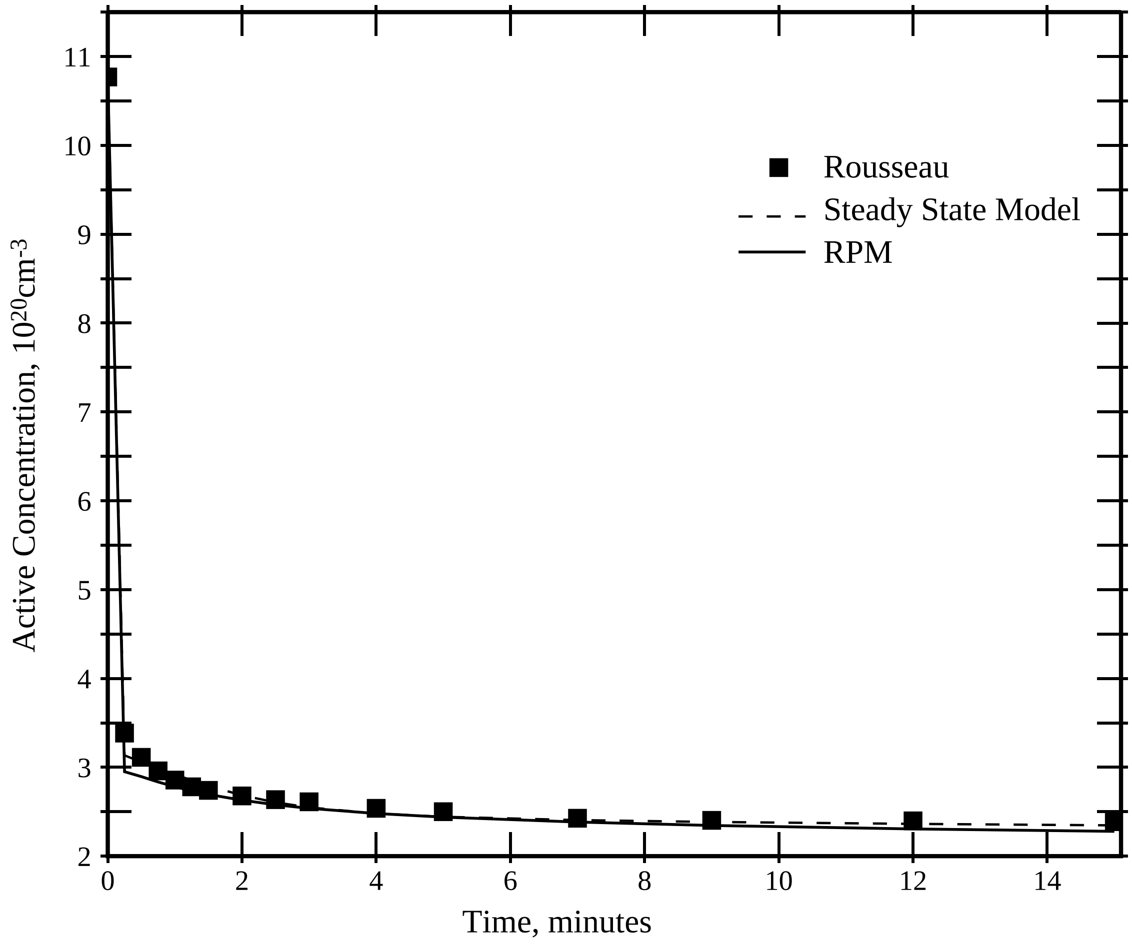

Figure 4: Clejan and Dunham

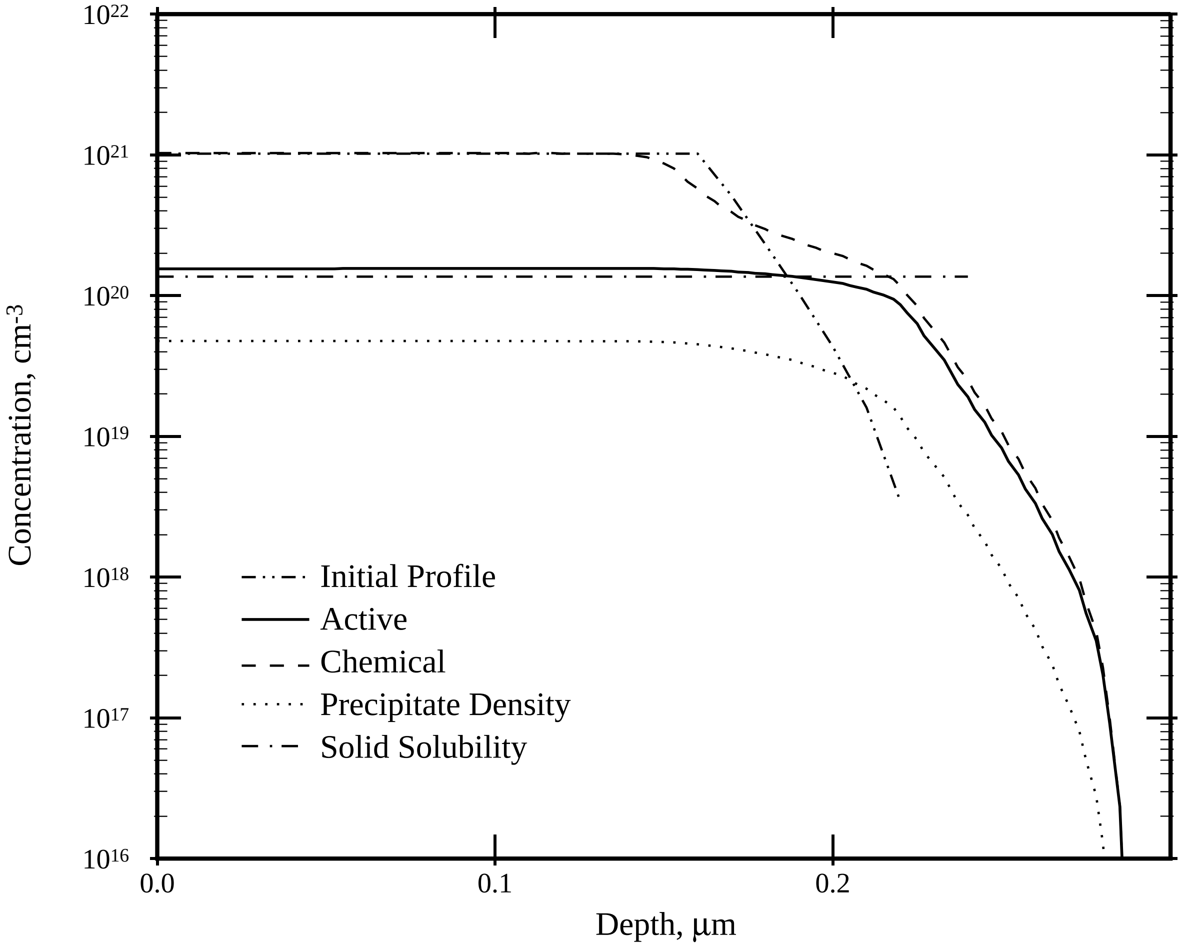

Figure 5: Clejan and Dunham

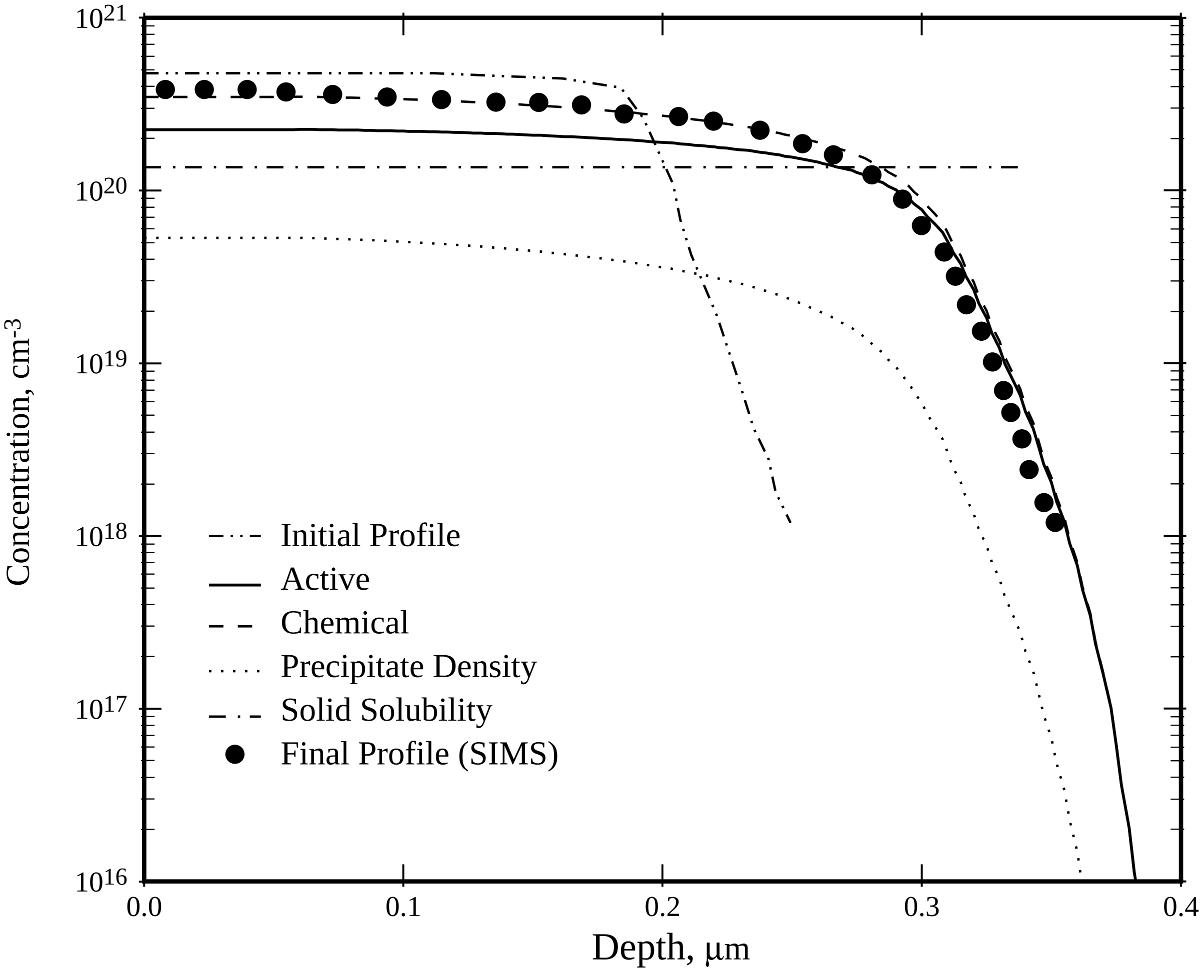

Figure 6: Clejan and Dunham

TABLE I. Parameters used in the simulations. Those parameters marked with references are from previously published results as indicated in the text. The remaining parameter values were determined based on optimizing the FKPM to precipitation data at 800°C and below. Parameters with Arrhenius temperature dependencies are assumed to be given by $A = A^0 \exp(-A^E/kT)$.

Parameter	Phosphorus	Arsenic
c_1 (eV)	0.63	0.21
c_2 (eV)	-1.20	0.15
c_3 (eV)	-0.43	0.02
D_0^0 (cm^2/sec)	1.06×10^{-4} [a]	0.06 [b]
D_0^E (eV)	2.54 [a]	3.44 [b]
D_-^0 (cm^2/sec)	2.51 [a]	12.0 [b]
D_-^E (eV)	3.73 [a]	4.05 [b]
D_H^0 (cm^2/sec)	6.45×10^{-8}	5.45×10^{-6} [c]
D_H^E (eV)	1.96	1.65 [c]
n_L	4.5 [c]	4.5 [c]

[a] See reference [13]
[b] See reference [12]
[c] See reference [15]